Size dependence of the contact angle of a nanodrop in a nanocavity: Density functional theory considerations

Gersh O. Berim[*] and Eli Ruckenstein

Department of Chemical and Biological Engineering, State University of New York at Buffalo, Buffalo, New York 14260, USA

The dependence of the contact angles of nanodrops of Lennard-Jones type fluids in nanocavities on their sizes are calculated using a nonlocal density functional theory in a canonical ensemble. Cavities of various radii and depths, various temperatures, as well as various values of the energy parameter of the fluid-solid interactions were considered. It is argued that this dependence might affect strongly, for instance, the rate of heterogeneous nucleation on rough surfaces, which is usually calculated under the assumption of constant contact angle.

I. INTRODUCTION

When a small liquid drop is in contact with a smooth homogeneous solid substrate it acquires the shape of a spherical cup, which creates with the solid surface a constant contact angle θ_Y provided by the Young equation $\cos\theta_Y = (\gamma_{sv} - \gamma_{ls})/\gamma_{lv}$, where γ_{sv}, γ_{ls}, and γ_{lv} are the surface tensions for substrate-vapor, substrate-liquid, and liquid-vapor interfaces, respectively. The angle θ_Y was also considered constant when the heterogeneous nucleation of a liquid from vapor was treated by considering the nucleus of the new phase as a uniform drop [1–4]. In the framework of the classical nucleation theory [1–3], this assumption essentially simplifies the calculation of the free-energy barrier for nucleation, which is a function of the unique contact angle given by the Young equation. In the kinetic theory of nucleation [5,6], the constancy of θ_Y simplifies the calculation of the evaporation and condensation rates, which are involved in the rate of nucleation.

However, as well known (see, for example, Refs. [7–12]), for small drops with sizes of several microns on a solid surface, the contact angle θ depends on the radius r of the contact line and hence θ depends on the size of the drop. In the classical theory of wetting, this dependence is accounted for by introducing the line tension τ in a modified Young equation $\cos\theta = \cos\theta_Y - \tau/\gamma_{lv}r$, where $1/r$ is the curvature of the contact line [7–12]. However, when the size of the drop is of the order of a few nanometers (as it is for a nucleus), the thicknesses of the fluid-liquid and fluid-solid interfaces become comparable to the size of the drop, and the classical concepts of surface tensions defined for bulk phases are not applicable. In such cases, the contact angle should be determined differently, on the basis of a microscopic theory. One such theory, the density functional theory (DFT) in a canonical ensemble, was successfully applied to the description of nanodrops on smooth planar solid surfaces as well as to droplike objects (bumps, bridges between walls of nanoslits, etc.) [13–18]. In this paper, DFT is employed to examine a nanodrop in a cavity of a solid surface, focusing on the dependence of the contact angle that the nanodrop makes with the wall of the cavity on the size of the drop. For the sake

of simplicity, two-dimensional (cylindrical) cavities and drops will be considered.

II. BACKGROUND

Let us consider a system of finite dimensions L_x and L_h in the x and h directions, respectively, and infinite dimension in the y direction, which contains a one-component fluid of fixed average density $\rho_{\rm av}$ in contact with a solid surface (see Fig. 1 where the y axis is normal to the plane of the figure). The solid contains a cylindrical cavity (groove) of radius R and depth d and is considered to have a uniform density ρ_s. The fluid density distribution (FDD) $\rho(\mathbf{r})$ in such a system is uniform in the y direction and nonuniform in the x and h directions, i.e., $\rho(\mathbf{r}) \equiv \rho(x,h)$. A periodic boundary condition is employed in the x direction, and the upper boundary of the box is treated as a hard wall.

The interactions between the fluid molecules and the fluid molecules and the solid substrate are considered of the Lennard-Jones type with a hard core repulsion $\phi(|\mathbf{r} - \mathbf{r}'|) = 4\epsilon[(\frac{\sigma}{r})^{12} - (\frac{\sigma}{r})^6]$ for $r \geqslant \sigma$ and $\phi(|\mathbf{r} - \mathbf{r}'|) = \infty$ for $r < \sigma$, where the coordinates $\mathbf{r}$ and $\mathbf{r}'$ provide the locations of the interacting molecules, $r = |\mathbf{r} - \mathbf{r}'|$, and σ and ϵ are the hard core diameter and the energy parameter, respectively. In the following, the notations ϵ_{ff}, σ_{ff} and ϵ_{fs}, σ_{fs} are used for fluid-fluid and fluid-solid interactions, respectively.

The total Helmholtz free energy $F[\rho(\mathbf{r})]$ of the fluid in the external potential generated by the solid, the Euler-Lagrange equation for FDD, and an outline of the numerical procedure used to solve the Euler-Lagrange equation are provided in Refs. [15] and in the Appendix.

A typical example of a two-dimensional FDD is presented in Fig. 2(a). To determine the profile of a drop on the basis of the obtained FDD, a procedure similar to that used in Refs. [15] was employed. First, the one-dimensional FDD along the h axis (vertical axis of symmetry) was determined from the two-dimensional FDD obtained by solving the Euler-Lagrange equation. An example of such a FDD is presented in Fig. 2(b). In the vicinity of the liquid-solid interface, there are strong density oscillations due to the ordering of the fluid molecules, which form several liquid layers of various densities. At larger distances from the solid, the density becomes almost constant, acquiring liquidlike values and then quickly decreasing across the liquid-vapor interface and
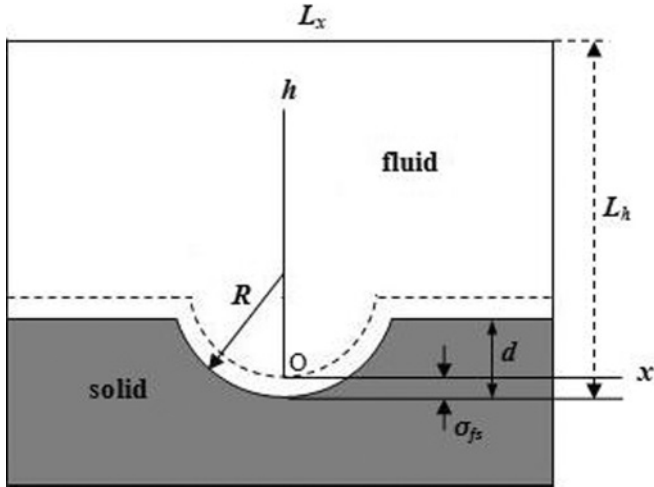
———————
[*]gberim@buffalo.edu

FIG. 1. Schematic presentation of the considered system, which is infinite in the y direction (normal to the plane of the figure) and is periodic with period L_x in the x direction. The dashed line indicates the location of the centers of the fluid molecules in the first (nearest to the solid) layer. Other notations are presented in the text.

approaching vaporlike values. Considering the AB range [see Fig. 2(b)] of the fluid density distribution, which contains the vapor-liquid interface, the location of the equimolar dividing surface and the corresponding density ρ_{div} were determined. The drop profile was extracted from the two-dimensional FDD as a curve along which the local fluid density has the value ρ_{div}. Note that a similar approach for calculating the contact angle was used in Refs. [19–21], where the FDDs were obtained by molecular dynamics simulations.

An example of a drop profile obtained as described above is presented schematically in Fig. 2(c) by the dotted line. Because of the complex structure of this profile near the solid surface, its upper part was approximated by a circle and extended up to the surface of the cavity. The angle θ that this circle makes with the surface of the cavity was considered as the actual contact angle. This procedure is similar to that used in the experimental determination of the contact angle. Note that the change of the location of the dividing surface and the corresponding change of ρ_{div} weakly affect the calculated contact angle. For

instance, a change of ρ_{div} by 10% with respect to that obtained for the equimolar dividing surface results in changes of the contact angle of about 0.5%. The size of the cylindrical drop is characterized by the number of molecules N_d it contains per unit length along the y direction of the drop. This number is provided by the expression $N_d = \int_S \rho(x,h)dx\,dh$, where S is the area between the cavity and the circle that approximates the drop profile. For convenience, the dimensionless quantity $N_d^* \equiv N_d \sigma_{ff}$, which typically has an order of magnitude of 10^2, will be used in the following. This quantity provides the number of molecules in a part of the cylindrical drop of length σ_{ff}.

Note that a droplike solution of the Euler-Lagrange equation can be obtained only if the average fluid density in the system is larger than $\rho_{\mathrm{av},d}$ which depends on the interaction potentials, the geometry of the system, and temperature. For $\rho_{\mathrm{av}} < \rho_{\mathrm{av},d}$, the fluid forms a film. Typically, $\rho_{\mathrm{av},d}\sigma_{ff}^3$ is between 0.04 and 0.05. The obtained droplike solutions are stable in closed systems but unstable in the open ones; similar features were noted for drops on a planar surface in Refs. [13,14] and for bridges and bubbles in cylindrical pores in Ref. [17].

III. RESULTS

In this study, argon was selected as the fluid; it has the interaction parameters $\epsilon_{ff}/k_B = 119.76$ K and $\sigma_{ff} = 3.405$ Å. The temperatures $T = 85$ and 95 K were selected. As a supporting solid, the solid carbon dioxide was considered with $\epsilon_{fs} = \epsilon_{fs}^0$ ($\epsilon_{fs}^0/k_B = 153.0$ K) and $\sigma_{fs} = 3.727$ Å [22]. To examine the effect of the fluid-solid interactions on the FDD in the cavity, other solids were considered, which differ from CO_2 only via the energy parameter ϵ_{fs}; all the other parameters remained unchanged. The width of the system L_x was taken as $L_x = 60\sigma_{ff}$ and the height as $L_h = 20\sigma_{ff} + 2\sigma_{fs}$. Two cavity radii $R_1 = 15\sigma_{ff}$ and $R_2 = 11\sigma_{ff}$ were selected with cavity depths $d_1 = 5\sigma_{ff}$ and $d_2 = 10\sigma_{ff}$, respectively. For comparison purposes, drops on a planar surface were also considered for the same parameters of the fluid-solid interactions.

The size dependence of the contact angle at $T = 85$ K is presented in Fig. 3 for various cavities and energy parameters ϵ_{fs}. The solid and dashed lines are for cavities with $R = 15\sigma_{ff}$ and $11\sigma_{fs}$, respectively. The curves for different ϵ_{fs}
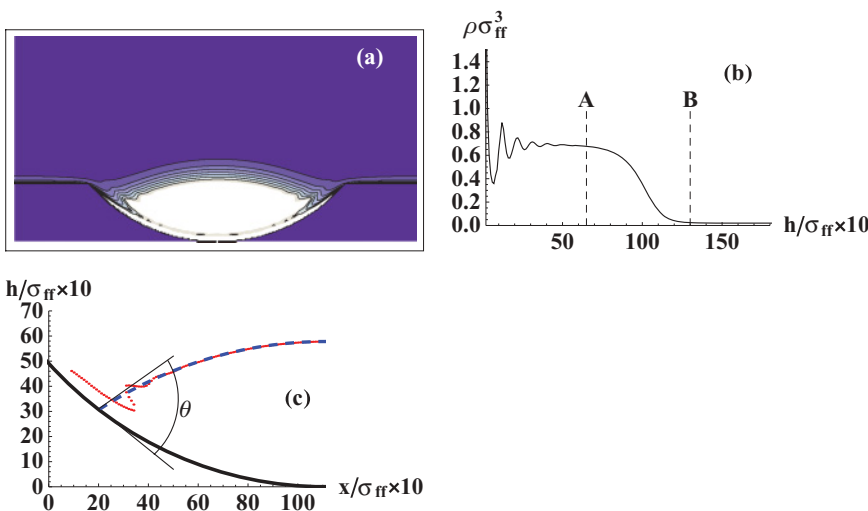

FIG. 2. (Color online) (a) Example of a two-dimensional fluid density distribution (FDD) in a cavity of radius $R = 15\sigma_{ff}$ and depth $d = 5\sigma_{ff}$. The lighter areas correspond to higher fluid densities. (b) One-dimensional FDD along the vertical axis of symmetry of the two-dimensional FDD presented in panel (a). The region AB contains the liquid-vapor interface. (c) Half of the drop profile (dotted line) extracted from the FDD of panel (a). The solid line is the surface of the cavity, and the dashed line represents the circular approximation of the upper part of the drop profile. θ is the contact angle.
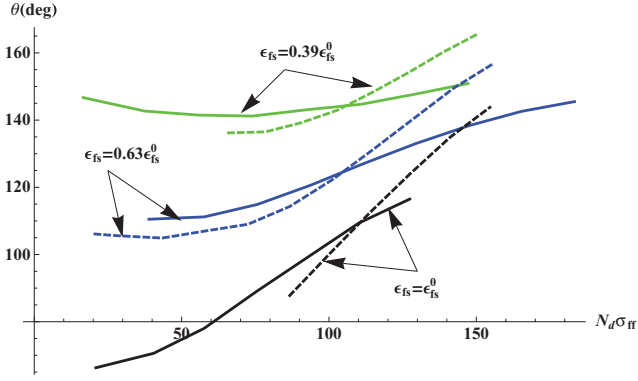
FIG. 3. (Color online) Size dependence of the contact angle in a cavity with $R = 15\sigma_{ff}$ (solid lines) and $R = 11\sigma_{ff}$ (dashed lines) for various values of the energy parameter ϵ_{fs} of the fluid-solid interactions.

in this figure are plotted for various drop sizes. The upper bounds $N_{d,\max}$ of these sizes correspond to the largest drops with the leading edge located inside the cavity. The lower bounds $N_{d,\min}$ correspond to the smallest drops that can be formed in the cavity. From Fig. 3, one can see that, in all cases, there is a considerable variation $\Delta\theta$ of the contact angle with the drop size. For example, for $\epsilon_{fs} = \epsilon_{fs}^0$ and $R = 15\sigma_{ff}$, the contact angle increases monotonously from $\theta = 66.3°$ to $116.5°$ ($\Delta\theta = 50.2°$) as N_d^* increases from 20.9 to 127.4, respectively. (The average fluid density in this case changes from $\rho_{av}\sigma_{ff}^3 = 0.042$ to $\rho_{av}\sigma_{ff}^3 = 0.124$.) Note that a nanodrop on a planar surface of the same solid makes with the surface a contact angle $\theta_{pl} \simeq 52°$, the change of the latter with the size being of the order of only a few degrees. The value of θ_{pl} is close to the value of θ for the smallest of the considered drops in the cavity. This is expected because the smallest drop in the cavity can be approximately considered as located on a planar surface.

For $\epsilon_{fs} = 0.39\epsilon_{fs}^0$ and $R = 15\sigma_{ff}$, the contact angle has a nonmonotonous dependence on the drop size with a much smaller variation $\Delta\theta$ ($\Delta\theta \sim 10°$) (Fig. 3). Such a behavior is the obvious consequence of the weaker fluid-solid interactions. The contact angle θ_{pl} for this case is $137°$, which is close to the values of θ for drops in the cavity.

For an intermediate value of the fluid-solid interactions ($\epsilon_{fs} = 0.63\epsilon_{fs}^0$ and $R = 15\sigma_{ff}$, $\theta_{pl} \sim 104°$) the contact angle changes from $\theta = 110.5°$ to $\theta = 138.3°$ ($\Delta\theta = 27.8°$) when N_d^* changes from 38.9 to 147.3 (Fig. 3). For the cavity

with $R = 11\sigma_{ff}$, the size dependence of the contact angle represented by the dashed curves of Fig. 3 is qualitatively the same as for the cavity with the larger radius ($R = 15\sigma_{ff}$). Comparing the behavior of the contact angle as function of the drop size N_d for cavities with $R = 15\sigma_{ff}$ and $R = 11\sigma_{ff}$, one can see that, for small N_d, the contact angle is smaller for the cavity with the smaller radius. However, this inequality is inverted as N_d increases (see Fig. 3). The inversion occurs for $N_d^* \simeq 10^2$. A summary of the results is provided in Table I where, instead of $\Delta\theta$, the average rate $\overline{\Delta\theta} \equiv \Delta\theta/(N_{d,\max}^* - N_{d,\min}^*)$ of the variation of $\Delta\theta$ with the change of the number of molecules in the drop is presented. As one can see from Table I, for a selected cavity, $\overline{\Delta\theta}$ decreases with decreasing ϵ_{fs} but increases with increasing temperature. For the same ϵ_{fs}, $\overline{\Delta\theta}$ increases with decreasing cavity radius.

It is of interest to note that the dependence of the contact angle of a drop on the cavity radius leads, at least in some cases, to a transition from nonwetting ($\theta > 90°$) to wetting ($\theta < 90°$) with decreasing cavity radius (increasing curvature of the surface). See, for example, the case with $\epsilon_{fs} = \epsilon_{fs}^0$ and $N_d^* < 90$ in Fig. 3. The opposite transition from wetting to nonwetting situations with increasing curvatures of the solid was predicted in Ref. [23], where a drop on a cylindrical fiber was considered.

It is instructive to examine the dependence of the contact angle that a drop of given size makes with the cavity on the cavity radius. The results of such calculations for a drop with $N_d^* = 130$ in a cavity of depth $5\sigma_{ff}$ are presented in Table II for various substrates (various $\epsilon_{fs}/\epsilon_{fs}^0$). One can see that the contact angle decreases with increasing cavity radius in the direction of the contact angle θ_{pl} of a drop on a planar surface, with the rate of change being the largest for smaller radii. However, even for the largest considered cavity radius $R = 90\sigma_{ff}$, the contact angle does not reach θ_{pl}. In our calculations, the consideration of cavity radii larger than $R = 90\sigma_{ff}$ was not possible because of the small size of the system selected to provide reasonable calculation times. Nevertheless, the results are compatible with the expected contact angle dependence on R.

IV. DISCUSSION

The obtained results show that the contact angle that a nanodrop makes with the surface of a cavity depends on the size N_d of the drop. This dependence becomes more pronounced with increasing ϵ_{fs}, increasing temperature and

TABLE I. Summary of results obtained for the size dependence of the contact angle Θ for a nanodrop in a nanocavity. All notations are explained in the text.

R	$\varepsilon_{fs}/\varepsilon_{fs}^0$	$T = 85$K			$T = 95$K		
		$N_{d,\min}\sigma_{ff}$	$N_{d,\max}\sigma_{ff}$	$\overline{\Delta\theta}$	$N_{d,\min}\sigma_{ff}$	$N_{d,\max}\sigma_{ff}$	$\overline{\Delta\theta}$
	1	20.9	127.4	0.471	38.5	91.6	0.683
$15\sigma_{ff}$	0.63	38.9	147.3	0.257	36.7	131.4	0.309
	0.39	16.6	147.2	0.074	35.3	112.9	0.084
	1	86.7	154.6	0.825	77.7	135.5	0.951
$11\sigma_{ff}$	0.63	20.6	156.3	0.376	66.3	140.1	0.633
	0.39	65.9	150.4	0.348	65.2	114.4	0.459

TABLE II. The contact angle for a drop with $N_{nd}{}^* = 130$ on various substrates and for various cavity radii.

R/σ_{ff}	$\varepsilon_{fs}/\varepsilon_{fs}{}^0$		
	0.39	0.63	1.0
15	147.7°	133.0°	117.0°
25	144.5°	115.3°	75.8°
45	144.2°	113.9°	71.2°
90	142.3°	114.1°	69.1°
planar surface	137.0°	104.0°	52.0°

decreasing cavity radius R. The dependence of the contact angle on the drop size can considerably affect the nucleation rate calculated both by the classical [1] and kinetic [5,6] nucleation theories. In both approaches, the size dependence of the contact angle affects the size dependence of the fluid-liquid and fluid-solid contact areas, which contribute to the free energy of nucleus and hence can change the size of the critical cluster and, as a consequence, the rate of nucleation. In the kinetic theory, in addition, the nonuniformity of the fluid density distribution inside the drop, which can affect the evaporation rate of molecules from the nucleus, should be taken into account.

Because of computational restrictions, the radii of the cavities and the sizes of the drops considered in this paper do not exceed 6–7 nm. Such sizes are much smaller than those for which one expects the classical theory of wetting to be valid. As shown in Refs. [16,24], where the capillary condensation in spherical pores was examined using the classical and the density functional approaches, these approaches provided similar results when the cavity radius was larger than 100 nm.

Note that, for nanodrops, in contrast to macrodrops, the contact angle on a smooth solid surface depends slightly on the size of the drop. For example, at $\epsilon_{fs} = 0.39\epsilon_{fs}^0$, this angle changes from $\theta_1 = 139.4°$ to $\theta_2 = 132.8°$ when the size of the base of the drop changes from $2.6\sigma_{ff} \simeq 9$ Å to $7.4\sigma_{ff} \simeq 25$ Å, and the number of molecules in the drop is changed from $N_d^* \simeq 25$ to $N_d^* \simeq 190$. However, the variation of the contact angle on the smooth surface is much smaller than that in the cavity (compare $\Delta\theta \simeq 7°$ for a planar surface with $\Delta\theta \simeq 35°$ for a cavity with radius $R = 11\sigma_{ff}$).

Note, in conclusion, that the results for the size dependence of the contact angle were obtained here for a cylindrical drop in a cylindrical cavity. However, as previously shown [25] for drops on a planar surface, the difference between the drop profiles of cylindrical and axisymmetrical ones is not large. Therefore, one can expect the size dependence of the contact angle obtained in this paper to remain valid for drops in spherical cavities as well.

APPENDIX: FREE-ENERGY CONTRIBUTIONS AND SOLUTION OF THE EULER-LAGRANGE EQUATION

The total Helmholtz free energy $F[\rho(\mathbf{r})]$ of a fluid in the external potential generated by a solid is expressed as the sum of an ideal gas free energy $F_{id}[\rho(\mathbf{r})]$, a free energy $F_{hs}[\rho(\mathbf{r})]$ of a reference system of hard spheres, a free energy $F_{attr}[\rho(\mathbf{r})]$ due to the attractive interactions between the fluid

molecules (in the mean-field approximation), and a free energy $F_{fs}[\rho(\mathbf{r})]$ due to the interactions between the fluid and solid. These contributions to the free energy can be represented as follows [26,27]:

$$F_{id}[\rho(\mathbf{r})] = k_B T \int d\mathbf{r}\, \rho(\mathbf{r})\{\log[\Lambda^3 \rho(\mathbf{r})] - 1\}, \quad (A1)$$

$$F_{hs}[\rho(\mathbf{r})] = \int d\mathbf{r}\, \rho(\mathbf{r})\Delta\Psi_{hs}(\mathbf{r}), \quad (A2)$$

where $\Lambda = h_P/(2\pi m k_B T)^{1/2}$ is the thermal de Broglie wavelength, h_P and k_B are the Planck and Boltzmann constants, respectively, T is the absolute temperature, m is the mass of a fluid molecule,

$$\Delta\Psi_{hs}(\mathbf{r}) = k_B T \eta_{\bar{\rho}}\frac{4 - 3\eta_{\bar{\rho}}}{(1 - \eta_{\bar{\rho}})^2}\,, \quad (A3)$$

$\eta_{\bar{\rho}} = \frac{1}{6}\pi\bar{\rho}(\mathbf{r})\sigma_{ff}^3$ is the packing fraction of the fluid molecules, σ_{ff} is the fluid hard core diameter, and $\bar{\rho}(\mathbf{r})$ is the smoothed density defined as

$$\bar{\rho}(\mathbf{r}) = \int d\mathbf{r}'\rho(\mathbf{r}')W(|\mathbf{r} - \mathbf{r}'|)\,. \quad (A4)$$

The weighting function $W(|\mathbf{r} - \mathbf{r}'|)$ is selected in the form [28]

$$W(|\mathbf{r} - \mathbf{r}'|) = \begin{cases} \frac{3}{\pi\sigma_{ff}^3}\left(1 - \frac{r}{\sigma_{ff}}\right), & r \leqslant \sigma_{ff} \\ 0, & r > \sigma_{ff} \end{cases}$$

where $r = |\mathbf{r} - \mathbf{r}'|$.

The contribution to the excess free energy due to the attraction between the fluid-fluid molecules is calculated in the mean-field approximation

$$F_{attr}[\rho(\mathbf{r})] = \frac{1}{2}\int\int d\mathbf{r}\, d\mathbf{r}'\rho(\mathbf{r})\rho(\mathbf{r}')\phi_{ff}(|\mathbf{r} - \mathbf{r}'|), \quad (A5)$$

where $\phi_{ff}(|\mathbf{r} - \mathbf{r}'|)$ is the potential of the fluid-fluid interactions.

The last contribution $F_{fs}[\rho(\mathbf{r})]$ is given by the expression

$$F_{fs}[\rho(\mathbf{r})] = \int_V d\mathbf{r}\, \rho(\mathbf{r})U_{fs}(\mathbf{r}), \quad (A6)$$

where V is the volume occupied by the fluid and $U_{fs}(\mathbf{r})$ is the net potential generated by the solid. This potential is given by

$$U_{fs}(\mathbf{r}) = \int_{V_s}\rho_s(\mathbf{r}')\phi_{fs}(|\mathbf{r} - \mathbf{r}'|)\, d\mathbf{r}', \quad (A7)$$

where $\phi_{fs}(|\mathbf{r} - \mathbf{r}'|)$ is the potential of the fluid-solid interactions, V_s is the volume of the solid, $\rho_s(\mathbf{r}')$ is the density of the solid, which, in general, depends on coordinates. Note that the integration over y and x coordinates in the three-dimensional integral of Eq. (A7) can be carried out in analytical form, whereas the integration over h can be performed only numerically.

The Euler-Lagrange equation for the fluid density distribution $\rho(x,h)$ obtained by minimizing the Helmholtz free energy can be represented in the following general form:

$$\log[\Lambda^3\rho(x,h)] - Q(x,h) = \frac{\lambda}{k_B T}, \quad (A8)$$

where λ is the Lagrange multiplier and the function $Q(x,h)$ is given by

$$Q(x,h) = -\frac{1}{k_B T}[\Delta\Psi_{hs}(x,h) + \overline{\Delta\Psi'}_{hs}(x,h) \\ + U_{ff}(x,h) + U_{fw}(x,h)], \quad (A9)$$

where

$$U_{ff}(x,h) \\ = \int\int dx' dh' \rho(x',h')\phi_{ff,y}(|x-x'|,|h-h'|), \quad (A10)$$

$$\overline{\Delta\Psi'}_{hs}(x,h) = \int\int dx' dh' \rho(x',h')W_y(|x-x'|,|h-h'|) \\ \times \frac{\partial}{\partial\bar{\rho}}\Delta\Psi_{hs}(\bar{\rho})|_{\bar{\rho}=\bar{\rho}(x',h')}, \quad (A11)$$

$\phi_{ff,y}(|x-x'|,|h-h'|)$ and $W_y(|x-x'|,|h-h'|)$ are obtained by integrating the potential $\phi_{ff}(|\mathbf{r}-\mathbf{r}'|)$ and the weighted function $W(|\mathbf{r}-\mathbf{r}'|)$ with respect to y from $-\infty$ to $+\infty$.

When calculating the term $U_{ff}(x,h)$ of the Euler-Lagrange equation arising due to the long-range fluid-fluid interactions, a cutoff at a distance equal to four molecular diameters σ_{ff} for the range of Lennard-Jones attraction was employed. The increase of this distance up to $10\sigma_{ff}$ changed the results by less than 1%.

In Eq. (A8), the Lagrange multiplier λ arises because of the constraint of fixed average density of the fluid, which has the form

$$\rho_{av} = \frac{1}{V}\int_V d\mathbf{r}\,\rho(\mathbf{r}) \quad (A12)$$

and leads to the following expression for λ :

$$\lambda = -k_B T \log\left(\frac{1}{\rho_{av}V\Lambda^3}\int_V d\mathbf{r}\,e^{Q(x,h)}\right). \quad (A13)$$

By eliminating λ between Eqs. (A8) and (A13), one obtains an integral equation for the FDD $\rho(x,h)$, which was solved by iteration.

The initial FDD in the iteration procedure (initial guess) was selected to be uniform inside the cavity, with a liquidlike density ($\rho\sigma_{ff}^3 \sim 0.5$). Outside the cavity, it was taken as uniform with a vaporlike density ($\rho\sigma_{ff}^3 \sim 0.04 \div 0.10$). By changing the fluid densities inside and outside the cavity in the initial guess (i.e., by changing the average density in the system), drops of various sizes could be obtained.

To avoid the divergence of the iteration procedure, the input density profile $\rho_i^{in}(x,h)$ for the $(i+1)$th iteration $\rho_{i+1}(x,h)$, generated by the Euler-Lagrange equation, was selected as follows [26]:

$$\rho_i^{in}(x,h) = (1-\gamma)\rho_{i-1}^{in}(x,h) + \gamma\rho_i(x,h), \quad (A14)$$

where $\rho_i(x,h)$ is the ith iteration and the constant $\gamma = 0.1$. As a measure of the precision of the iterations, the dimensionless quantity

$$\delta = \int_V dx\,dh\big[\rho_{i+1}(x,h) - \rho_i^{in}(x,h)\big]^2 / \left(\int_V dx\,dh\,\rho_i(x,h)\right)^2$$

was introduced. The iterations were carried out on a two-dimensional grid with a spacing equal to $0.1\sigma_{ff}$ until δ became smaller than $\epsilon = 10^{-7}$. The additional increase in precision did not lead to appreciable changes in the density profile.

[1] Q. X. Liu, Y. J. Zhu, G. W. Yang, and Q. B. Yang, J. Mater. Sci. Technol. **24**, 183 (2008).

[2] S. J. Cooper, C. E. Nicholson, and J. Liu, J. Chem. Phys. **129**, 124715 (2008).

[3] M. Qian and J. Ma, J. Chem. Phys. **130**, 214709 (2009).

[4] E. Ruckenstein and G. O. Berim, J. Colloid Interface Sci. **355**, 259 (2011).

[5] B. Nowakowski and E. Ruckenstein, J. Phys. Chem. **96**, 2313 (1992).

[6] E. Ruckenstein and B. Nowakowski, Langmuir **8**, 1470 (1992).

[7] J. Gaydos and A. W. Neumann, J. Colloid Interface Sci. **120**, 76 (1987).

[8] F. Y. H. Lin, D. Li, and A. W. Neumann, J. Colloid Interface Sci. **159**, 86 (1993).

[9] L. Schimmele, M. Napiorkowski, and S. Dietrich, J. Chem. Phys. **127**, 164715 (2007).

[10] A. Checco, P. Guenoun, and J. Daillant, Phys. Rev. Lett. **91**, 186101 (2003).

[11] A. Marmur, J. Colloid Interface Sci. **186**, 462 (1997).

[12] A. Marmur, Colloids Surf. A **136**, 81 (1998).

[13] V. Talanquer and D. W. Oxtoby, J. Chem. Phys. **104**, 1483 (1996).

[14] V. Talanquer and D. W. Oxtoby, J. Chem. Phys. **114**, 2793 (2001).

[15] G. O. Berim and E. Ruckenstein, J. Chem. Phys. **129**, 014708 (2008).

[16] A. V. Neimark, P. I. Ravikovitch, and A. Vishnyakov, Phys. Rev. E **65**, 031505 (2002).

[17] A. Vishnyakov and A. V. Neimark, J. Chem. Phys. **119**, 9755 (2003).

[18] F. Ancilotto, M. Barranco, E. S. Hernandez, A. Hernando, and M. Pi, Phys. Rev. B **79**, 104514 (2009).

[19] C. D. Daub, J. Wang, S. Kudesia, D. Bratko, and A. Luzar, Faraday Discuss. **146**, 67 (2010).

[20] N. Giovambattista, P. G. Debenedetti, and P. J. Rossky, J. Phys. Chem. B **111**, 9581 (2007).

[21] M. J. de Ruijter, T. D. Blake, and J. De Coninck, Langmuir **15**, 7836 (1999).

[22] R. Evans and P. Tarazona, Phys. Rev. A **28**, 1864 (1983).

[23] A. V. Neimark, J. Adhes. Sci. Technol. **13**, 1137 (1999).

[24] P. I. Ravikovitch and A. V. Neimark, Langmuir **18**, 1550 (2002).

[25] G. O. Berim and E. Ruckenstein, J. Phys. Chem. B **108**, 19330 (2004).

[26] P. Tarazona, Phys. Rev. A **31**, 2672 (1985).

[27] P. Tarazona *et al.*, Mol. Phys. **60**, 573 (1987).

[28] R. H. Nilson and S. K. Griffiths, J. Chem. Phys. **111**, 4281 (1999).